

Unconventional Non-Fermi Liquid Properties of Two-Channel Anderson Impurities System

Atsushi Tsuruta¹ and Kazumasa Miyake²

¹Division of Materials Physics, Department of Materials Engineering Science, Graduate School of Engineering Science, Osaka University, Toyonaka, Osaka 560-8531, Japan

²Center for Advanced High Magnetic Field Science, Osaka University, Toyonaka, Osaka 560-0043, Japan

E-mail: tsuruta@mp.es.osaka-u.ac.jp

April 2021

Abstract. A theory for treating the unconventional non-Fermi liquid temperature dependence of physical quantities, such as the resistivity, in the Pr-based two-channel Anderson impurities system is developed. It is shown that their temperature dependences are essentially the same as those in the pure lattice system except for the case of extremely low concentration of Pr ions that is difficult to realize by the controlled experiments. This result is consistent with recent observations in diluted Pr-1-2-20 system $\text{Y}_{1-x}\text{Pr}_x\text{Ir}_2\text{Zn}_{20}$ ($x = 0.024, 0.044, 0.085$, and 0.44) reported in Yamane *et al.* Phys. Rev. Lett. **121**, 077206 (2018), and is quite different from that in the case of single-channel Anderson impurities system in which the crossover between behaviors of the local Fermi liquid and heavy Fermi liquid occurs at around moderate concentration of impurities as observed in Ce-based heavy fermion system $\text{La}_{1-x}\text{Ce}_x\text{Cu}_6$.

1. Introduction

In a past decade, non-Fermi liquid behaviors observed in the so-called Pr-1-2-20 compounds, $\text{PrT}_2\text{A}_{20}$ ($T=\text{Ti, V; Rh, Ir}$ and $A=\text{Al; Zn}$), have attracted much attention [1, 2, 3, 4]. Namely, the temperature (T) dependence of the electrical resistivity follows \sqrt{T} -like behavior in a wide T region. The specific heat, $C(T)$, and the magnetic susceptibility, $\chi_m(T)$, increase in proportion to $(\text{const.} - \sqrt{T})$ toward T_Q , the transition temperature of quadrupolar ordering, as T decreases below the Kondo temperature T_K that is a fundamental energy scale characterizing the physics. Similar anomalies have been reported in PrPb_3 [5]. The common aspect of these compounds is that the ground state of the crystalline-electrical field (CEF) of the localized 4f-electron in Pr^{3+} ion is the Γ_3 non-Kramers doublet in $4f^2$ -configuration, as verified by analyses of the specific heat and the magnetic moment, and inelastic neutron scattering experiments [3].

Such a system with the Γ_3 CEF ground state in f^2 -configuration is expected to exhibit anomalous behaviors associated with the two-channel Kondo effect [6, 7, 8, 9]. Indeed, we have shown that the above mentioned anomalous properties can be understood in a unified fashion on the basis of the two-channel Anderson lattice model [10], with the use of $1/N$ expansion method *à la* Nagoya group [12, 13, 14, 15] that makes it possible to take into account the strong correlation effect properly by

satisfying a series of constraints among auxiliary particles, slave fermions and bosons, in each order of $1/N$. In particular, the T dependence of the resistivity $\rho(T)$ is given in the form [10]

$$\rho(T) = \frac{aT}{T + bT_0} \left(1 - \frac{1}{M^2}\right) + c \left(\frac{T}{T_K}\right)^2, \quad (1)$$

where M is the number of channel, and T_0 is the temperature characterizing the non-Fermi liquid state below which the \sqrt{T} -like dependence in the resistivity is observed in wide T region although the resistivity follows the T -linear dependence in the low temperature limit $T \ll T_0$. Note that this T_0 is a new temperature scale characterizing the two-channel lattice Anderson or Kondo system which should be distinguished from the so-called Kondo temperature T_K for the single-channel lattice Anderson or Kondo system. The coefficients a and c in Eq. (1) are constants with dimension of the resistivity, and depend on the materials parameters characterizing the system, such as the strength of the c-f hybridization. On the other hand, b is approximately given by $b \simeq 0.67$ as discussed in Appendix A. It is crucial that the non-Fermi liquid term scaled by T_0 in Eq. (1) exists only in the case of multi-channel with $M \geq 2$. This scaling behavior has really been observed in a series of Pr-1-2-20 compounds with different T_0 s depending on the pressure and the magnetic field [16, 17]. The relationship between the scaling form given by Eq. (1) and the scaling behaviors observed in Refs. [16, 17] is discussed in Appendix A.

On the other hand, it has been reported recently in diluted systems $Y_{1-x}\text{Pr}_x\text{Ir}_2\text{Zn}_{20}$ ($x = 0.024, 0.044, 0.085, 0.44$) [18] that the T dependence in the resistivity $\rho(T)$ follows essentially the same as that of the lattice system, i.e., $x = 1$. This contradicts the theoretical result for the two-channel ($M = 2$) impurity Kondo effect [11] according to which $\rho(T) \propto (\text{const.} \pm \sqrt{T})$ depending whether the exchange interaction is in the strong coupling region (+) or weak coupling region (-). If the system is located in the strong-coupling region, observed T -dependence could be understood as the two-channel impurity Kondo effect. However, since it is rather hard to expect that these systems are located in the strong coupling region, this conflicting behavior cannot be understood as the two-channel impurity Kondo effect, offering theorists a big challenge.

In this paper, we show theoretically that the two-channel Anderson impurities system as $Y_{1-x}\text{Pr}_x\text{Ir}_2\text{Zn}_{20}$ ($10^{-6} \lesssim x \ll 1$) exhibits essentially the same non-Fermi liquid behaviors as the pure system with $x = 1$ unless x is extremely small less than $x^{\text{cr}} \sim 10^{-6}$ for a reasonable set of parameters. The organization of the present paper is as follows. In Sect. 2, the model for the two-channel Anderson impurities system is introduced, and an outline of the $1/N$ -expansion method for taking the strong correlation effect is recapitulated. In Sect. 3, a new formalism of treating the effect of random distribution of dilute Pr ions is proposed. In Sect. 4, on the basis of the formalism developed in Sect. 3, the T dependence of the resistivity in the two-channel Anderson impurities system is derived. In Sect. 5, the T dependence of physical quantities is summarized. In Sect. 6, the critical impurity concentration $c_{\text{imp}}^{\text{cr}}(x^{\text{cr}})$ below which the resistivity shows the T dependence of the single impurity model is discussed, showing that $c_{\text{imp}}^{\text{cr}}$ for the two-channel model is extremely small of $\mathcal{O}(10^{-6})$ and not reached by controlled experiments, while that for the single-channel model is only moderately smaller than 1 in consistent with observation in Ce-based impurity heavy fermion systems such as $\text{Ce}_x\text{La}_{1-x}\text{Cu}_6$ [19, 20].

2. Model Hamiltonian and Formulation

A canonical model for describing Pr-1-2-20 compounds, in which the CEF ground state of Pr^{3+} ion in $4f^2$ configuration is the Γ_3 non-Kramers doublet and hybridizing with conduction electrons with Γ_8 symmetry leaving the $4f^1$ Γ_7 Kramers doublet (as shown in Fig. 1), is given by the two-channel Anderson lattice model discussed in Refs. [13, 14, 10]:

$$\begin{aligned}
 H_{2\text{cAL}} = & \sum_{\sigma=1}^M \sum_{\tau_1, \tau_2=1}^N \sum_{\mathbf{k}} \varepsilon_{\mathbf{k}\tau_1\tau_2} c_{\mathbf{k}\tau_1\sigma}^+ c_{\mathbf{k}\tau_2\sigma} \\
 & + \sum_i \sum_{\tau=1}^N \varepsilon_{\Gamma_3}^{(0)} b_{i\tau}^+ b_{i\tau} + \sum_i \sum_{\sigma=1}^M \varepsilon_{\Gamma_7}^{(0)} f_{i\sigma}^+ f_{i\sigma} \\
 & + \frac{1}{\sqrt{N_L}} \sum_{\sigma=1}^M \sum_{\tau=1}^N \sum_{i, \mathbf{k}} \left(V c_{\mathbf{k}\tau\sigma}^+ b_{i\tau} f_{i\sigma}^+ e^{-i\mathbf{k} \cdot \mathbf{R}_i} + \text{h.c.} \right), \quad (2)
 \end{aligned}$$

where $c_{\mathbf{k}\tau\sigma}$ is the annihilation operators of a conduction electron with wave vector \mathbf{k} and dispersion $\varepsilon_{\mathbf{k}\tau_1\tau_2}$, and spin-orbital component σ (with $\bar{\sigma}$ being the opposite component of σ) specifying the CEF ground state of Γ_8 in the $4f^1$ configuration ($M = 2$), $b_{i\tau}$ is that of the pseudo boson representing the i -th localized f^2 state of energy $\varepsilon_{\Gamma_3}^{(0)}$ with the symmetry of Γ_3 with quadrupole moment τ ($N = 2$), $f_{i\sigma}$ is that of the pseudo fermion representing the i -th localized f^1 state of energy $\varepsilon_{\Gamma_7}^{(0)}$ with spin-orbital momentum σ specifying the CEF ground state of Γ_7 , and V represents the hybridization transforming from the f^2 -state with τ at i -th site to the composite state of f^1 with σ at the same site and that described by $c_{\mathbf{k}\tau\bar{\sigma}}$, and vice versa, as shown in Fig. 1. Note that N_L is the total number of lattice sites for conduction electrons while the f-electrons occupy only the sites of Pr ions that is dilutely distributed on the N_L lattice sites, and $N = 2$ and $M = 2$ stand for components of the spin-orbital degeneracy and that of the quadrupole moment, respectively. Hereafter, we discard $\varepsilon_{\mathbf{k}\tau\bar{\tau}}$, which is non zero in general, because there occurs no qualitative difference from the case $\varepsilon_{\mathbf{k}\tau\bar{\tau}} \neq 0$ as described in Ref. [10].

To guarantee that the transformed model [Eq. (2)] describes the physical process shown in Fig. 1, the Hamiltonian [Eq. (2)] must be treated within the subspace where the local constraint

$$\hat{Q}_i = \sum_{\tau} b_{i\tau}^+ b_{i\tau} + \sum_{\sigma} f_{i\sigma}^+ f_{i\sigma} = 1, \quad (3)$$

is fulfilled. To calculate physical quantities within the subspace restricted by the local constraint [Eq. (3)], we evaluate the expectation value $\langle \hat{A} \rangle$ of a physical quantity \hat{A} such that [21, 22]

$$\langle \hat{A} \rangle = \lim_{\{\lambda_i\} \rightarrow \infty} \left(\langle \hat{A} \Pi_i \hat{Q}_i \rangle_{\lambda} / \langle \Pi_i \hat{Q}_i \rangle_{\lambda} \right), \quad (4)$$

where

$$\langle \hat{A} \Pi_i \hat{Q}_i \rangle_{\lambda} \equiv \text{Tr}[e^{-\beta H_{\lambda}} \hat{A} \Pi_i \hat{Q}_i] / Z_{\lambda}, \quad (5)$$

with

$$Z_{\lambda} \equiv \text{Tr}[e^{-\beta H_{\lambda}}], \quad (6)$$

$$H_{\lambda} \equiv H + \sum_i \lambda_i \hat{Q}_i. \quad (7)$$

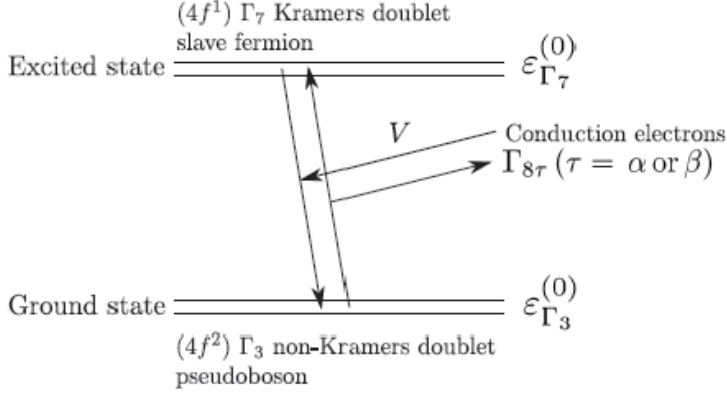


Figure 1. Levels scheme of f-electrons and hybridization path with conduction electrons of model Hamiltonian [Eq. (2)].

In order to calculate the average [Eq. (4)] explicitly, we employ the perturbation expansion in the power of $1/N$ following the rules as

$$\frac{1}{N_L} \sum_{\tau} \sum_{\mathbf{k}} 1 = O[(1/N)^0], \quad (8)$$

and

$$\frac{1}{N_L} \sum_{\mathbf{k}} 1 = O(1/N). \quad (9)$$

In Refs. [12, 15], one can see the validity of this rule of power counting in $1/N$ and its physical meaning behind it. For explicit calculations in this paper, we set $N = 2$, which may not lose the generality because we do not use the condition $1/N \ll 1$ explicitly.

3. Average over Random Distribution of Pr Ions

A basic idea is that 4f electrons at Pr sites acquire the wave vector \mathbf{p} dependence through the average process over the random distribution of Pr ions, which in turn gives rise to two contributions to the scattering process of the conduction electrons, i.e., a single site effect of localized f-electrons and the lattice effect due to the wave-number dependent collective quadrupole fluctuations [23].

To estimate the effect of scattering due to the random distribution of Pr ions, we have to take an average over their random distribution. Before taking the average, the one-particle Green function of f-electrons depends on the two positions as $G_f(\mathbf{r}_i, \mathbf{r}_j; i\varepsilon_n)$, where $i\varepsilon_n$ is the fermionic Matsubara frequency, but it becomes a function of the relative coordinate $(\mathbf{r}_i - \mathbf{r}_j)$ after taking the average over the random distribution of Pr ions so that the Green function acquires the wave vector representation in general. This kind of procedure has been established in the case where the conduction electrons are influenced by the random distribution of impurities giving random potential, as discussed, e.g., in the textbook [24]. However, this acquirement of the diagonal wave vector dependence or the recovery of translational symmetry is only due to a general property of the random average. Namely, this is

not an approximation, but is based on the principle or "Ansatz" of physical statistics. In this sense, it is virtually rigorous. In fact, the uniformity of the distribution of Pr impurities was confirmed experimentally with good accuracy at least in the case of $\text{Y}_{1-x}\text{Pr}_x\text{Ir}_2\text{Zn}_{20}$ [18, 25]. Therefore, by taking this average, the wave vector dependent Green function becomes well defined as

$$\bar{G}_{\bar{\mathbf{f}}}(\mathbf{p}, i\varepsilon_n) = \sum_{(i-j)} e^{-i\mathbf{p}\cdot(\mathbf{r}_i-\mathbf{r}_j)} \langle\langle G_{\mathbf{f}}(\mathbf{r}_i, \mathbf{r}_j; i\varepsilon_n) \rangle\rangle, \quad (10)$$

where $\langle\langle \dots \rangle\rangle$ denotes the average over the random distribution of Pr ions. By the inverse Fourier transformation, we can introduce the real space *image* behind the expression [Eq. (10)] as shown in Fig. 2(b) in which Pr ions are distributed regularly in a certain plane, e.g. xy plane, on a *virtual* lattice assumed to be simple cubic for simplicity. However, there exists no direct (or one-to-one) correspondence between positions of lattice points of the original and *virtual* lattice because the origin of the *virtual* lattice cannot be fixed by the inverse Fourier transformation that specifies only the dependence on the relative coordinate $(\mathbf{r}_i - \mathbf{r}_j)$. This is consistent with the fact that the average number of Pr ions at the original lattice point becomes uniform after the average over the random distributions of Pr ions.

As discussed below, with the use of this *virtual lattice* system, the temperature dependence of the damping rate of quasiparticles, consisted of Pr impurities, can be estimated relying on the theory for periodic lattice system developed in Ref. [10] which explains quite well existing experimental facts in a unified way. As a result, transport properties observed in diluted Pr-1-2-20 systems can be understood consistently.

Since the mean distance between localized 4f electrons is given by $(N_L/N_f)^{1/3}a$, with a and N_f being the lattice constant of the original lattice and the total number of localized 4f electrons of Pr ions, we can introduce the real space *image* behind the expression [Eq.(10)] as given by Fig. 2(b) in which Pr ions are distributed regularly on a *virtual* lattice. Namely, an expression of the wave vector \mathbf{p} is given by

$$\mathbf{p} = \frac{2\pi}{L}(n_x, n_y, n_z) \quad (11)$$

where the integer n_α ($\alpha = x, y, z$) is restricted as $0 \leq |n_\alpha| \leq (N_L/N_f)^{1/3}/2$, L is the length of one side of the cubic material and N_f is the number of Pr ions in the original lattice system. However, we have not assumed that the Pr ions form a periodic lattice in the *original* lattice in Fig. 2(a). Therefore, of course, this periodicity in the *virtual* lattice cannot be observed by diffraction methods, X-ray and/or neutron scattering, in the *real* crystal. Hereafter, \mathbf{p} 's are used for the wave vectors in the *virtual* lattice obtained after the random average over the positions of Pr ions, and are distinguished from wave vectors \mathbf{k} 's in the original lattice shown in Fig. 2(a).

On the other hand, conduction electrons described by wave vector \mathbf{p} are essentially unaltered by the effect of scattering by Pr impurities except for some broadening of the dispersion due to impurities scattering [24]. Namely, for example, the density of states (DOS) of conduction electrons at the Fermi level are essentially unaltered. However, since the size of the Brillouin zone (BZ) of the *virtual* lattice is shortened by a factor $c_{\text{imp}}^{1/3}$, the band of conduction electrons splits into multibands in the shortened and reduced BZ [26]. However, hereafter for simplicity of presentation, we use an extended zone scheme for conduction electrons.

Thus, we can discuss physical properties of the 2-channel Anderson lattice system on the *virtual* periodic lattice described by the *virtual* Hamiltonian for the *virtual*

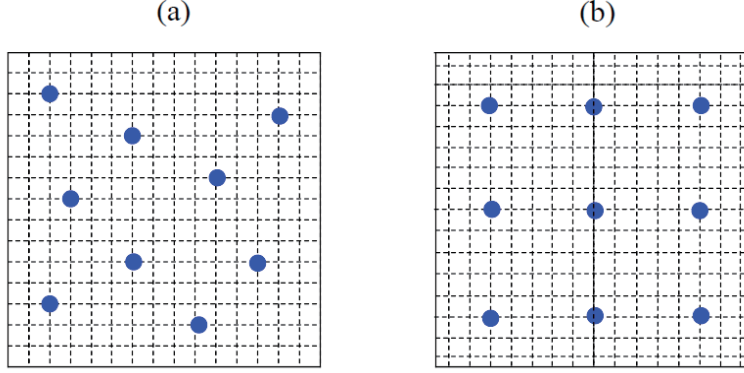


Figure 2. (a) Square lattice version of original system where the sites occupied by Pr ions are shown by filled circle. (b) *Virtual* system obtained after average over random distribution of Pr sites. Hereafter, conduction electrons are assumed to be described by wave vector \mathbf{p} in both systems.

lattice shown in Fig. 2(b). The *virtual* Hamiltonian $H_{2\text{cAL}}^{\text{v}}$ is given explicitly as follows:

$$\begin{aligned}
 H_{2\text{cAL}}^{\text{v}} \equiv & \sum_{\sigma=1}^N \sum_{\tau_1, \tau_2=1}^M \sum_{a, \mathbf{p}} \varepsilon_{a\mathbf{p}\tau_1\tau_2} \tilde{c}_{a\mathbf{p}\tau_1\sigma}^+ \tilde{c}_{a\mathbf{p}\tau_2\sigma} \\
 & + \sum_{\tilde{i}}^M \sum_{\tau=1}^M \varepsilon_{\Gamma_3}^{(0)} \tilde{b}_{i\tau}^+ \tilde{b}_{i\tau} + \sum_{\tilde{i}}^N \sum_{\sigma=1}^N \varepsilon_{\Gamma_7}^{(0)} \tilde{f}_{i\sigma}^+ \tilde{f}_{i\sigma} \\
 & + \frac{1}{\sqrt{N_{\text{L}}}} \sum_{\sigma=1}^N \sum_{\tau=1}^M \sum_{\tilde{i}, a, \mathbf{p}} \left(V \tilde{c}_{a\mathbf{p}\tau\sigma}^+ \tilde{b}_{i\tau} \tilde{f}_{i\sigma}^+ e^{-i\mathbf{p} \cdot \mathbf{R}_{\tilde{i}}} + \text{h.c.} \right) \\
 & + \sum_{\tilde{i}, \sigma} u_{\text{imp}} P_{\tilde{i}} n_{i\sigma}^{\tilde{c}}
 \end{aligned} \tag{12}$$

where $\tilde{c}_{a\mathbf{p}\tau\sigma}$ and $\tilde{f}_{i\sigma}$ are the annihilation operators of conduction electrons at band a and f electrons at \tilde{i} -th site in the *virtual* periodic lattice, respectively, and $n_{i\sigma}^{\tilde{c}}$ is the numbers of conduction at \tilde{i} -th site ($\tilde{i} = 1, 2, \dots, N_{\text{f}}$). Note that the factor $1/\sqrt{N_{\text{L}}}$ in the 4th term of Eq. (12) reflects the fact that the f electrons are located on the periodic *virtual* lattice points of N_{f} while the conduction electrons are hopping among the original lattice points of N_{L} as discussed in Appendix B. The random variables $P_{\tilde{i}}$ in the last term of Eq. (12) represent the distribution of the strength of impurity scattering and arises from the random distribution of Pr ions on the original lattice shown in Fig. 2(a). With the use of this *virtual* Hamiltonian, the theoretical framework for discussing the two-channel Anderson lattice system can be applied as it stands except the effect of impurities scattering on conduction electrons [10].

In $\text{PrIr}_2\text{Zn}_{20}$, Zn atoms form icosahedral cages with cubic (T_d) symmetry around Pr atoms. Even in the case of dilute Pr atoms in $\text{Pr}_x\text{Y}_{1-x}\text{Ir}_2\text{Zn}_{20}$ ($x \ll 1$), the symmetry of the 4f electrons contained in the Pr atom is basically determined by the local Zn icosahedral cage around the Pr atom. Therefore, the ground state of the CEF of the f-electron in the Pr atom is considered to remain basically as Γ_3 , while the cage containing Pr atoms may be slightly distorted due to the effect of

the other cages containing Pr atoms that are dilute and randomly located around the Pr atom in attention. However, the distortion is small enough because the cage is rigid and x is small enough in the system in question, so that the effect is negligible in the zeroth-order approximation. As circumstantial evidence, the T dependence of the electrical resistivity in the Pr dilute system reported in Ref. [18] shows basically the same non-Fermi liquid T dependence as that of the system with $x = 1$. This is also consistent with the following experimental fact. Indeed, the T dependence of ultrasound dispersion in the same system shows that the width of the energy splitting of Γ_3 states, Δ_{Γ_3} , is about 0.048K [28], which is sufficiently lower than the characteristic temperature scale characterising the non-Fermi liquid state: $T_0 = 0.3\text{K}$ [18], above which the T dependence of the electrical resistivity deviates from \sqrt{T} behavior. It is obvious that if Δ_{Γ_3} is larger than T_0 , the non-Fermi liquid temperature dependence disappears. On this observation, we consider that Δ_{Γ_3} is small enough, giving no essential effect. In this sense, we have assumed that $\Delta_{\Gamma_3} = 0$. We consider that this assumption is correct at $x \sim 1$ and $x \ll 1$ where non-Fermi liquid behaviors have been observed in experiments [18], while in the intermediate region we can not ignore the effect of breaking the cubic symmetry.

Concluding this section, we compare our theoretical framework, which takes into account the effect of the impurity scattering on the conduction electrons from randomly distributed f-electrons, with three traditional methods for alloy systems discussed in Ref. [27].

(1) Our method of introducing the *virtual lattice* proposed in the present paper is different from the “virtual crystal approximation (VCA)”, which is the method used for a homogeneous model in which the parameters contained in the Hamiltonian are averaged by concentration of alloy. For example, the VCA cannot describe the existence of the hybridization gap caused by the c-f hybridization when applied to the non-interacting Anderson model. In the model that assumes a simple virtual crystal without f-f interaction, it is impossible to discuss how the effect of the local correlation between f-electrons influences on the T dependence of the electrical resistivity. The *virtual lattice* in the present paper should be distinguished from VCA.

(2) Our method shares in part a common aspect with the “averaged t-matrix approximation (ATA)”, which is a good approximation in the dilute region of f-electrons. For example, the problem associated with the hybridization gap mentioned above in (1) is cleared as far as in the dilute case of f-electrons where the direct f-f hopping is safely neglected. However, we need to extend it further, to capture the effect of the local correlation between f-electrons and the scattering effect by randomly distributed f-electrons that is the origin of the resistivity. In that sense, the method proposed in the present paper can be regarded as one of reasonable extensions of ATA.

(3) There is no restriction on the concentration of f-electrons, c_{imp} , in the framework of the present paper, in contrast to the “coherent potential approximation (CPA)”, in which the c-f hybridization gap disappears where the direct f-f hopping is neglected in the dilute region as mentioned above in (2). Indeed, the theoretical result, obtained by the CPA with the dynamical mean field theory (DMFT), does not seem to reproduce the Nordheim rule $\rho \propto x(1 - x)$ observed in $\text{Ce}_x\text{La}_{1-x}\text{Cu}_6$ [19] in the dilute case $x = c_{\text{imp}} < 0.3$ [29].

4. Dual Nature of Resistivity

The original one-particle Green function $G_c(\mathbf{r}_i, \mathbf{r}_j; i\varepsilon_n)$ of conduction electrons satisfies the Dyson equation as

$$G_c(\mathbf{r}_i, \mathbf{r}_j; i\varepsilon_n) = G_c^{(0)}(\mathbf{r}_i, \mathbf{r}_j; i\varepsilon_n) + \sum_{k, \ell} G_c^{(0)}(\mathbf{r}_i, \mathbf{r}_k; i\varepsilon_n) \Sigma_c(\mathbf{r}_k, \mathbf{r}_\ell; i\varepsilon_n) G_c(\mathbf{r}_\ell, \mathbf{r}_j; i\varepsilon_n), \quad (13)$$

where $G_c^{(0)}(\mathbf{r}_i, \mathbf{r}_j; i\varepsilon_n)$ is the non-interacting Green function of conduction electrons, and $\Sigma_c(\mathbf{r}_k, \mathbf{r}_\ell; i\varepsilon_n)$ is the self-energy arising from the hybridization between the f-electrons at Pr sites. Here, we have abbreviated the suffices σ and τ specifying the spin-orbital and quadrupole degrees of freedom for the concise presentation. After taking the average over the random distribution of Pr ions, both the Green function and the self-energy depend only on the relative coordinate $(\mathbf{r}_i - \mathbf{r}_j)$'s and acquire the wave vector representation. Namely, the Green function $\bar{G}_{\bar{c}}(\mathbf{p}, i\varepsilon_n) \equiv \sum_{(i-j)} e^{-i\mathbf{p} \cdot (\mathbf{r}_i - \mathbf{r}_j)} \langle \langle G_c(\mathbf{r}_i, \mathbf{r}_j; i\varepsilon_n) \rangle \rangle$ satisfies the Dyson equation as

$$\bar{G}_{\bar{c}}(\mathbf{p}, i\varepsilon_n) = G_c^{(0)}(\mathbf{p}, i\varepsilon_n) + G_c^{(0)}(\mathbf{p}, i\varepsilon_n) \bar{\Sigma}_{\bar{c}}(\mathbf{p}, i\varepsilon_n) \bar{G}_{\bar{c}}(\mathbf{p}, i\varepsilon_n), \quad (14)$$

where $G_c^{(0)}(\mathbf{p}, i\varepsilon_n)$ is the Green function of free band electrons on the original lattice, and the self-energy $\bar{\Sigma}_{\bar{c}}(\mathbf{p}, i\varepsilon_n)$ is defined by

$$\bar{\Sigma}_{\bar{c}}(\mathbf{p}, i\varepsilon_n) \equiv \sum_{(i-j)} e^{-i\mathbf{p} \cdot (\mathbf{r}_i - \mathbf{r}_j)} \langle \langle \Sigma_c(\mathbf{r}_i, \mathbf{r}_j; i\varepsilon_n) \rangle \rangle. \quad (15)$$

The T dependence of the resistivity is essentially given by the imaginary part of the retarded function of $\bar{\Sigma}_{\bar{c}}(\mathbf{p}, i\varepsilon_n)$ [Eq. (15)], in which $\langle \langle \Sigma_c(\mathbf{r}_i, \mathbf{r}_j; i\varepsilon_n) \rangle \rangle$ consists of two parts as

$$\langle \langle \Sigma_c(\mathbf{r}_i, \mathbf{r}_j; i\varepsilon_n) \rangle \rangle = -\frac{i}{2\tau_{\text{imp}}} \text{sgn}(\varepsilon_n) \delta_{ij} + \langle \langle \Delta \Sigma_c(\mathbf{r}_i, \mathbf{r}_j; i\varepsilon_n) \rangle \rangle, \quad (16)$$

where $i/2\tau_{\text{imp}}$ represents the damping effect arising from independent static scattering by localized f electrons at site \mathbf{r}_i , and gives temperature- and energy-independent term to the resistivity that is proportional to the concentration c_{imp} of Pr ions on the original lattice shown in Fig. 2(a). The second part of Eq. (16) arises from the scattering in the two-channel Anderson lattice system described by the *virtual* Hamiltonian [Eq. (12)]. Namely, the Green function of conduction electrons $\bar{G}_{\bar{c}}(\mathbf{p}, i\varepsilon_n)$ has the following structure:

$$\bar{G}_{\bar{c}}(\mathbf{p}, i\varepsilon_n) = \left[i\varepsilon_n - \xi_{\mathbf{p}} + \frac{i}{2\tau_{\text{imp}}} \text{sgn}(\varepsilon_n) - \tilde{V}^2 \bar{G}_{\bar{f}}(\mathbf{p}, i\varepsilon_n) \right]^{-1}, \quad (17)$$

where \tilde{V} is the averaged c-f hybridization $\tilde{V} = \sqrt{c_{\text{imp}}} V$ as discussed in Appendix B (see Eq. (B.4)), and $\bar{G}_{\bar{f}}(\mathbf{p}, i\varepsilon_n)$ is the f-electron Green function given by the *virtual* Hamiltonian [Eq. (12)] so that it is influenced also by the damping effect of the conduction electrons as discussed below.

From the structure of the Green function of conduction electron [Eq. (17)], one can see that there exist two contributions to the resistivity. One arises from the renormalized impurity scattering of conduction electrons. Another one arises from the scattering in the two-channel Anderson lattice system described by the *virtual* Hamiltonian [Eq. (12)]. The latter is expected to have the same temperature

dependence of the resistivity as that of the lattice system except for the residual part at $T = 0$, i.e.,

$$\rho_{\text{lattice}}(T) - \rho_0^* \simeq \frac{aT}{T + bT_0} \left(1 - \frac{1}{M^2}\right) + c \left(\frac{T}{T_K}\right)^2, \quad (18)$$

which is essentially the same as Eq. (1) as shown below because it is essentially independent of the impurity scattering rate $1/2\tau_{\text{imp}}$ of conduction electrons. The residual resistivity ρ_0^* represents the renormalized resistivity arising from the renormalized impurities scattering rate $1/2\tilde{\tau}_{\text{imp}} \equiv 1/2\tau_{\text{imp}} + [-\text{Im}\langle\langle\Sigma_c^R(k_F^*, T=0)\rangle\rangle]$, where $\langle\langle\Sigma_c^R(k_F^*, T=0)\rangle\rangle$ is the imaginary part of the self-energy of conduction electrons in the *virtual* system described by the Hamiltonian [Eq. (12)].

The self-energies of conduction electrons in the *virtual* system consist of three parts, $\Sigma_c^{(a)}$, $\Sigma_c^{(b)}$, and $\Sigma_c^{(c)}$, as shown in Fig. 3, in which $\Sigma_c^{(a)}$ represents the effect of the two-channel Anderson impurity model, $\Sigma_c^{(b)}$ the local effect from the lattice contribution given by the d -infinity lattice model, and $\Sigma_c^{(c)}$ the contribution from the correction of the local vertex Γ_{loc} , which is crucial in the finite dimensional two-channel Anderson lattice model as discussed in Ref. [10]. The T dependence of the imaginary part of these self-energies with the lowest correction in T/\tilde{E}_0 are given in Appendix C as follows:

$$\text{Im}\Sigma_c^{(a)R}(\varepsilon=0; T) = -\tilde{C} \left[1 - 2\tilde{a}_f(T/\tilde{E}_0)^\nu \left(1 - \frac{1}{M^2}\right)\right] + A_{\text{imp}}T^2 \quad (19)$$

$$\text{Im}\Sigma_c^{(b)R}(\varepsilon=0; T) = \tilde{C} \frac{1}{M^2} \quad (20)$$

$$\text{Im}\Sigma_c^{(c)R}(\varepsilon=0; T) = \tilde{C} \frac{1 - 2\tilde{a}_f(T/\tilde{E}_0)^\nu \frac{\tilde{T}^*}{T} \left(1 - \frac{1}{M^2}\right)}{1 + \frac{\tilde{T}^*}{T}} - A_{\text{latt}}T^2, \quad (21)$$

where $\nu \equiv (1 - \tilde{a}_f)M/N$ [31], and the explicit expressions of coefficients \tilde{C} , \tilde{a}_f , \tilde{E}_0 , \tilde{T}^* , A_{imp} , and A_{latt} are derived on the basis of discussion in relation to Eq. (40) in Ref. [10] and that in Appendix C. However, it is crucial to note that the wave vector \mathbf{p} is defined on the *virtual* lattice of the *virtual* system described by the Hamiltonian [Eq. (12)] so that the hybridization is modified as $\tilde{V} \equiv \sqrt{c_{\text{imp}}}V$ as discussed in Appendix B. Namely, the hybridization in the *virtual* system should be replaced by \tilde{V} when we apply the results obtained in Ref. [10]. It is also crucial that \mathbf{k} -summation, $(1/N_L)\sum_{\mathbf{k}}$, in Ref. [10] should be replaced by $(1/N_f)\sum_{\mathbf{p}}$, i.e.,

$$\frac{1}{N_L}\sum_{\mathbf{k}} F(\mathbf{k}) \Rightarrow \frac{1}{N_f}\sum_{\mathbf{p}} F(\mathbf{p}) = \frac{1}{c_{\text{imp}}N_L}\sum_{\mathbf{p}} F(\mathbf{p}) \quad (22)$$

for an arbitrary function of $F(\mathbf{p})$.

The coefficient \tilde{C} in Eqs. (19)-(21) is given by Eq. (C.8) in Appendix C:

$$\tilde{C} = \frac{\pi}{N} \left(\frac{\tilde{a}_f\tilde{V}^2}{\tilde{E}_0}\right)^2 \tilde{N}(0), \quad (23)$$

where $\tilde{N}(0)$ is the spectral weight of conduction electrons defined by

$$\tilde{N}(0) \equiv -\frac{1}{\pi} \frac{1}{N_f} \sum_{\mathbf{p}, \tau} \text{Im}\tilde{G}_{c\tau\sigma}^R(\mathbf{p}, 0), \quad (24)$$

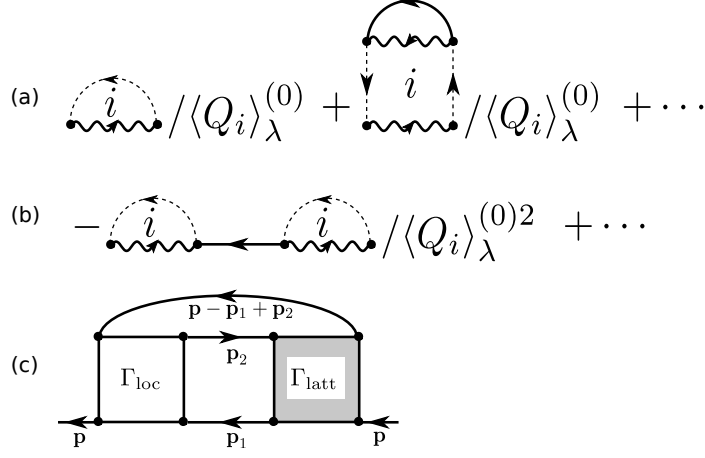


Figure 3. Self-energies of conduction electrons in the *virtual* system shown in Fig. 2(b). Solid lines, dotted lines, and wavy lines represent the Green functions of conduction electrons, pseudo bosons, and slave fermions, respectively, and filled circles are the c-f hybridization $\tilde{V} = \sqrt{c_{\text{imp}}}V$. (a) Self-energy for the impurity model corresponding to the *virtual* model [Eq.(12)]. The first and second terms represent the effect of $\mathcal{O}[(1/N)^0]$ and $\mathcal{O}[(1/N)^1]$, respectively, and the explicit form of higher order terms (dotted parts) are given by Eq. (4.6) in Ref. [30] representing the contribution of Fig. 4 in Ref. [30]. (b) Self-energy for the local effect arising from the *d*-infinity *virtual* model [Eq.(12)] of the order of $\mathcal{O}[(1/N)^1]$ given by Fig. 7(b) in Ref. [14]. The explicit forms of higher order terms (dotted parts) are given by Figs. 8(c)-8(f) and Figs. 9(c)-9(m) in Ref. [14]. (c) Self-energy from the lattice effect beyond the contribution from the local vertex Γ_{loc} given by the *virtual* two-channel Anderson lattice model [Eq.(12)]. Its explicit form is essentially the same as that given in Ref. [10] except that the hybridization shown by dot $\tilde{V} = \sqrt{c_{\text{imp}}}V$ has been modified in the *virtual* lattice system, and that the wave-vectors are defined on the *virtual* lattice. The structure of the renormalized vertex Γ_{latt} is discussed in Appendix C.

as derived from Eq. (40) in Ref. [10]. With the use of Eq. (22), $\tilde{N}(0)$ [Eq. (24)] is given as

$$\tilde{N}(0) = -\frac{1}{\pi} \frac{1}{c_{\text{imp}} N_L} \sum_{\mathbf{p}, \tau} \text{Im} \bar{G}_{\tilde{c}\tau\sigma}^{\text{R}}(\mathbf{p}, 0) \equiv \frac{N(0)}{c_{\text{imp}}}. \quad (25)$$

Therefore, \tilde{C} [Eq. (23)] is proportional to c_{imp} considering the relation $\tilde{V}^2 = c_{\text{imp}} V^2$, because \tilde{a}_{f} and \tilde{E}_0 are independent of c_{imp} as discussed below.

The residue \tilde{a}_{f} of the slave fermions in Eqs. (19) and (21) is given by Eq. (48) in Ref. [10] as

$$\frac{1}{\tilde{a}_{\text{f}}} = 1 + \frac{\tilde{V}^2}{N_{\text{f}}} \sum_{\mathbf{p}, \tau} \int d\varepsilon f(\varepsilon) \frac{-1}{\pi} \text{Im} \bar{G}_{\tilde{c}\tau\sigma}(\mathbf{p}, \varepsilon) \frac{1}{(\varepsilon - \tilde{E}_0)^2}, \quad (26)$$

where $f(\varepsilon)$ is the Fermi distribution function $f(\varepsilon) \equiv 1/(e^{\varepsilon/T} + 1)$.

The binding energy \tilde{E}_0 of the slave fermions appearing in Eqs. (19) and (21) is equivalent to the so-called Kondo temperature T_K , and is given as a solution of the

following equation derived in Ref. [10] [see Eq. (47)]

$$\varepsilon_{\Gamma_3} - \varepsilon_{\Gamma_7} - \tilde{E}_0 - \frac{\tilde{V}^2}{N_f} \sum_{\mathbf{p}, \tau} \int d\varepsilon f(\varepsilon) \frac{-1}{\pi} \text{Im} \tilde{G}_{c\tau\sigma}^R(\mathbf{p}, \varepsilon) \frac{1}{\varepsilon - \tilde{E}_0} = 0. \quad (27)$$

In Eqs. (26) and (27), σ dependence of \tilde{a}_f and \tilde{E}_0 has been abbreviated because we are considering the para-magnetic state.

The characteristic temperature \tilde{T}^* in Eq. (21) is given by

$$\tilde{T}^* = \frac{\tilde{E}_0}{1 + \tilde{N}(0)\tilde{E}_0} \left[1 - 2\tilde{a}_f(T/\tilde{E}_0)^\nu \right], \quad (28)$$

where the first factor in the limit $T = 0$ was derived in Ref. [10] [see Eq. (59) and the following description], and the second factor in the bracket is derived in Appendix C [Eq. (C.29)]. In the low T region, $T \ll \tilde{E}_0(0)$, \tilde{T}^* is approximated by

$$\tilde{T}^* \approx \frac{\tilde{E}_0(0)}{1 + \tilde{N}(0)\tilde{E}_0(0)}, \quad (29)$$

which is the factor bE_0 in Eq. (59) of Ref. [10].

With the use of \tilde{C} [Eq. (23)], as discussed in Appendix C [Eq. (C.13)], the coefficient A_{imp} in Eq. (19) is given by

$$A_{\text{imp}} \approx \frac{\pi^2}{3} \tilde{C} [1 - \tilde{a}_f(0)][2 + \tilde{a}_f(0)] \frac{1}{[\tilde{E}_0(0)]^2}, \quad (30)$$

while the coefficient A_{latt} in Eq. (21) is given, as discussed in Appendix C [Eq. (C.21)] by

$$A_{\text{latt}} \approx \frac{\pi}{4} \tilde{C}^2 N \frac{\tilde{a}_f(0)}{[\tilde{E}_0(0)]^3} \frac{1}{M}, \quad (31)$$

where $\tilde{a}_f(0)$ and $\tilde{E}_0(0)$ are those values at $T = 0$.

Note here that \tilde{C} is proportional to c_{imp} as discussed just below Eq. (25), and that \tilde{a}_f and \tilde{E}_0 are independent of c_{imp} as discussed below. Therefore, the coefficient A_{imp} [Eq. (30)] is proportional to c_{imp} reflecting the impurity effect, while the coefficient A_{latt} [Eq. (31)] is proportional to $[c_{\text{imp}}]^2$. This $[c_{\text{imp}}]^2$ dependence of A_{latt} can be understood from the structure of the Feynman diagram shown in Fig. 3(c). Namely, two internal wave-vectors summations give a factor $[c_{\text{imp}}]^{-2}$ according to the rule of Eq. (22) while eight hybridizations \tilde{V}^8 give a factor $[c_{\text{imp}}]^4$ because of the relation $\tilde{V} = \sqrt{c_{\text{imp}}} V$ in the *virtual* system. This result is also plausible because the Feynman diagram of Fig. 3(c) represents the effect of inter-site of Pr ions in the original lattice shown in Fig. 2(a) and is considered to be proportional to the product of probability c_{imp} of Pr ions in the original lattice system.

Adding the contributions [Eqs. (19)-(21)] together with the weak damping effect by static scattering of conduction electrons by localized f electrons at Pr sites, the imaginary part of the retarded self-energy of the conduction electrons $\text{Im} \Sigma_c^R(\varepsilon = 0; T)$ is given as

$$\begin{aligned} \text{Im} \Sigma_c^R(\varepsilon = 0; T) = & -\tilde{C} \left[1 - 2\tilde{a}_f(T/\tilde{E}_0)^\nu \right] \frac{T}{T + \tilde{T}^*} \left(1 - \frac{1}{M^2} \right) \\ & + A_{\text{imp}} T^2 - A_{\text{latt}} T^2 - \frac{1}{2\tilde{\tau}_{\text{imp}}}, \end{aligned} \quad (32)$$

where $1/2\tilde{\tau}_{\text{imp}}$ is the impurity scattering rate of the conduction electrons renormalized by the lattice effect in general, although it is essentially unrenormalized as discussed in Sect. 5.

The c_{imp} dependence of the above coefficients is important for the discussions below, and is given as follows. First of all, \tilde{a}_f and \tilde{E}_0 are independent of c_{imp} . This is because equations determining these quantities, Eqs. (26) and (27), are transformed to Eqs. (48) and (47) in Ref. [10], respectively, considering that $\tilde{V} = \sqrt{c_{\text{imp}}}V$ and the relation Eq. (22) holds. Since \tilde{a}_f and \tilde{E}_0 are independent of c_{imp} , the coefficient A_{imp} [Eq. (30)] is proportional to c_{imp} while the coefficient A_{latt} [Eq. (31)] is proportional to $[c_{\text{imp}}]^2$, as mentioned above. On the other hand, \tilde{T}^* given by Eq. (29) has no simple power-law dependence on c_{imp} . Indeed, using the expression for $\tilde{N}(0)$ [Eq. (25)], \tilde{T}^* [Eq. (29)] is reduced to

$$\tilde{T}^* \approx \frac{c_{\text{imp}}\tilde{E}_0(0)}{c_{\text{imp}} + N(0)\tilde{E}_0(0)}. \quad (33)$$

Namely, $\tilde{T}^* \approx c_{\text{imp}}/N(0) \sim c_{\text{imp}}/N_F$ in the low concentration limit of Pr ions, i.e., $c_{\text{imp}} \lesssim N(0)\tilde{E}_0(0)$, while $\tilde{T}^* \sim \tilde{E}_0(0)$ in a wide range of concentration $c_{\text{imp}} \gtrsim N(0)\tilde{E}_0(0) \sim N_F\tilde{E}_0(0)$ which is far smaller than 1 because $\tilde{E}_0(0) \sim T_K$ is far smaller than the Fermi energy E_F of conduction electrons in the present situation.

5. Temperature Dependence of Physical Quantities

In this section, we discuss the T dependence of various physical quantities.

With the use of $\text{Im}\Sigma_c^R(\varepsilon = 0; T)$ [Eq. (32)], the T dependence of the resistivity is essentially given by

$$\rho(T) = -\frac{2m}{N_e e^2} \text{Im}\Sigma_c^R(\varepsilon = 0; T), \quad (34)$$

where m and N_e are the mass of the free electron and the number density of conduction electrons, respectively, and we have assumed that the dispersion of conduction electrons is given by that of the free electron. Therefore, the T dependent part is essentially the same as that of the bulk pure system except for the c_{imp} dependence arising from the factor $\tilde{C} \propto c_{\text{imp}}$ and \tilde{T}^* [Eq. (33)] [32]. This is because the effect of the bare impurity scattering rate $1/2\tau_{\text{imp}}$ in the Green function of conduction electrons [Eq. (17)] does not alter the fundamental structure of T dependence in $\text{Im}\Sigma_c^R(\varepsilon = 0; T)$ [Eq. (32)]. Therefore, the so-called scaling behavior of the T dependence in $[\rho(T) - \rho_0^*]$, i.e., that given by Eq. (18), is expected to hold in the rather wide temperature region $T < \tilde{T}^*$ as in bulk pure systems [10].

One might think that the residual part at $T = 0$ K given by $\text{Im}\Sigma_c^R(\varepsilon = 0; 0)$, the renormalized scattering rate $1/2\tilde{\tau}_{\text{imp}}$ in Eq. (32), gives some additional residual resistivity other than that from $1/2\tau_{\text{imp}}$. However, we have verified that $\tilde{\tau}_{\text{imp}}$ is not influenced by a direct numerical calculation of $\text{Im}\Sigma_c^R(\varepsilon = 0; T = 0)$. In the case of the Anderson model with the zero interaction between f-electrons, $U_{ff} = 0$, $1/2\tilde{\tau}_{\text{imp}} \propto c_{\text{imp}}(1 - c_{\text{imp}})$ because of Nordheim rule. Even if we increase U_{ff} adiabatically, the c_{imp} dependence of $1/2\tilde{\tau}_{\text{imp}}$ does not change. In the numerical calculation in §6,

The chemical potential $\mu(T)$ and the specific heat $C_V(T)$ are also expected to exhibit the same T dependence as the bulk pure system because they are essentially

determined by the *virtual* Hamiltonian [Eq. (12)]. Namely, they are expected to exhibit the following T dependence in the region $T_Q < T \lesssim \tilde{E}_0$, with T_Q being the transition temperature of the quadrupole ordering [10]:

$$\mu(T) \propto \text{const.} - \sqrt{T}, \quad (35)$$

and

$$C_V(T) \propto \text{const.} - \sqrt{T}. \quad (36)$$

Such a T dependence in the specific heat does not contradict the observation in $\text{Y}_{1-x}\text{Pr}_x\text{Ir}_2\text{Zn}_{20}$ ($x = 0.024, 0.044, 0.085$, and 0.44). This is because the data on the T dependence reported in Ref. [18] can be fitted also by the functional form of Eq. (36) in the finite T range, although they fitted them by $C(T) \propto -T \log T$ [33].

6. Difference from Single-Channel Kondo Impurities System

As discussed in the previous sections, the T dependence of the resistivity in the two-channel Anderson impurities model is clearly different from that of the single-impurity two-channel Kondo [8, 9] or Anderson model [30] in which the resistivity is proportional to $(\text{const.} - \sqrt{T})$ toward $T = 0$ in the weak-coupling case [11]. On the other hand, in the present case, the resistivity arising from $\text{Im}\Sigma_c^R(\varepsilon = 0; T)$ [Eq. (32)] does not increase toward $T = 0$ even though there exists a factor $[1 - 2\tilde{a}_f(T/\tilde{E}_0)^\nu]$ that gives the non-Fermi liquid behavior expected in the single-impurity two-channel Kondo effect [30, 31]. Indeed, the quantity $[-\text{Im}\Sigma_c^R(0, T) + \text{Im}\Sigma_c^R(0, 0)]/Dc_{\text{imp}}$ in Eq. (32), which is proportional to the resistivity, for the parameter set, $\tilde{V}/D = 0.3$, $(\varepsilon_{\Gamma_3} - \varepsilon_{\Gamma_7})/D = -0.4$, $\tilde{E}_0/D = 0.0117$, and $\tilde{a}_f = 0.115$, is shown in Fig. 4 for a series of c_{imp} . One can see that the scaling behavior in T dependence of $[\rho(T) - \rho_0^*]/c_{\text{imp}}$ [Eq. (18)] holds down to the low concentration $c_{\text{imp}} \simeq 0.001$ less than that attained experimentally so far [18].

This is because the presence of a factor $T/(T + \tilde{T}^*)$ in Eq. (32) invalidates the increase in the resistivity, given by the factor $[1 - 2\tilde{a}_f(T/\tilde{E}_0)^\nu]$, in the low T region $T < \tilde{T}^*$. Therefore, in order that the single-impurity behavior is observed, \tilde{T}^* should be extremely small, e.g., $\tilde{T}^* = 0.01$ K which is a typical lower limit of T in the standard low temperature measurements using the dilution refrigerator. By solving approximate relation [Eq. (33)], the concentration c_{imp} is expressed by a function of \tilde{T}^* as

$$c_{\text{imp}} \approx \frac{\tilde{T}^* N(0) \tilde{E}_0(0)}{\tilde{E}_0(0) - \tilde{T}^*}. \quad (37)$$

Since $\tilde{E}_0(0)$ or the Kondo temperature T_K is of the order of 10 K in a conventional heavy fermion system, and $N(0) \sim 1/D$ with D being half the bandwidth of conduction electrons of the order of 10^4 K in a typical metal, the critical concentration $c_{\text{imp}}^{\text{cr}}$, below which the $[1 - 2\tilde{a}_f(T/\tilde{E}_0)^\nu]$ like T dependence in the resistivity is expected to be observed around $T \gtrsim \tilde{T}^* \sim 10^{-2}$ K, is roughly estimated as

$$c_{\text{imp}}^{\text{cr}} \sim \frac{\tilde{T}^*}{D} \sim 10^{-6}, \quad (38)$$

where we have neglected \tilde{T}^* compared to $\tilde{E}_0(0)$ in the denominator of (Eq. (37)) because we are interested in the case where $\tilde{T}^* \sim 10^{-2}$ K. Thus, it is extremely difficult to

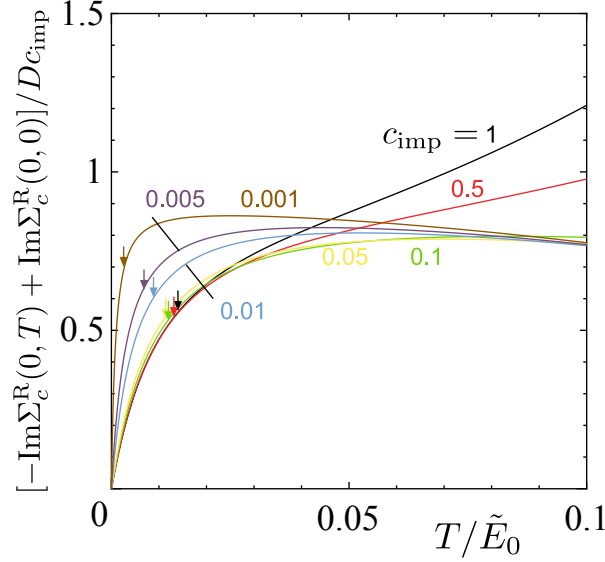


Figure 4. $[-\text{Im}\Sigma_c^R(0, T) + \text{Im}\Sigma_c^R(0, 0)]$ in Eq. (32) as a unit of Dc_{imp} for $M = 2$ and the parameter set, $\tilde{V}/D = 0.3$, $(\epsilon_{\Gamma_3} - \epsilon_{\Gamma_7})/D = -0.4$, $\tilde{E}_0/D = 0.0117$, and $\tilde{a}_f = 0.115$, as a function of T/\tilde{E}_0 for a series of $c_{\text{imp}} = 1 \sim 0.001$. Arrows indicate the temperature below which \sqrt{T} -like behavior appears down to $T = \tilde{T}^*$.

observe experimentally the non-Fermi liquid T dependence of the resistivity predicted on the single-impurity two-channel Kondo effect [8, 9].

The physical reason for this extremely small $c_{\text{imp}}^{\text{cr}}$ may be traced back to the character of the two-channel Kondo effect in which the local moment cannot be effectively screened out with the finite range of $\mathcal{O}(aD/T_K)$ with a being the mean distance among conduction electrons, but is over-screened unlike in the case of the single-channel Kondo effect [6, 34], resulting in the screening length (if any) diverges or extremely long compared to the case of the single-channel Kondo effect.

This situation is in marked contrast to the case of the single-channel ($M = 1$) Kondo or Anderson impurities model in which the T dependence of the resistivity at $T \ll T_K$ follows $(\text{const.} - T^2)$ dependence up to the relatively large concentration $c_{\text{imp}}^{\text{cr}} \sim 0.5$ of f-ions, e.g., Ce, as observed in $\text{Ce}_x\text{La}_{1-x}\text{Cu}_6$ [19, 20]. The difference stems from that of the M^2 dependence in the expression [Eq. (32)]. Namely, the anomalous T dependence with $M \geq 2$ disappears in the case of single-channel with $M = 1$. Therefore, Eq. (32) is reduced to

$$\text{Im}\Sigma_c^R(\epsilon = 0; T) = (A_{\text{imp}} - A_{\text{latt}})T^2 - \frac{1}{2\tilde{\tau}_{\text{imp}}}. \quad (39)$$

It is crucial to note that A_{imp} is proportional to c_{imp} while A_{latt} is proportional to $[c_{\text{imp}}]^2$ as Eqs. (30) and (31), respectively, because \tilde{C} [Eq. (23)] is proportional to c_{imp} . This implies that, in the low concentration region ($c_{\text{imp}} \ll 1$), the sign of T^2 term in $\text{Im}\Sigma_c^R(\epsilon = 0; T)$ is positive or the sign of T^2 term in $\rho(T)$ is negative, which leads to the local-Fermi liquid behavior [35]. On the other hand, in the high concentration region ($c_{\text{imp}} \lesssim 1$), the heavy Fermi liquid behavior is realized. This aspect is consistent with the observation reported in Ref. [20].

The critical concentration $c_{\text{imp}}^{\text{cr}}$, which separates the two Fermi liquid behaviors, is given by the condition $A_{\text{imp}} = A_{\text{latt}}$. Namely, by equating the expressions A_{imp} [Eq. (30)] and A_{latt} [Eq. (31)], with the use of Eqs. (23) and (25) and the relation $\tilde{V} = \sqrt{c_{\text{imp}}} V$, it is given as

$$c_{\text{imp}}^{\text{cr}} \approx \frac{8}{3} \left(\frac{\tilde{E}_0(0)}{\tilde{a}_f(0)V^2} \right)^2 \frac{1}{N(0)} \frac{\tilde{E}_0(0)}{\tilde{a}_f(0)}, \quad (40)$$

where we have approximated as $[1 - \tilde{a}_f(0)][2 + \tilde{a}_f(0)] \approx 2$ in the expression of A_{imp} [Eq. (30)] because $\tilde{a}_f(0) \ll 1$. Since $\tilde{E}_0(0) \sim \tilde{a}_f(0)V^2/D$ so that $\tilde{E}_0(0)/\tilde{a}_f(0) \sim V^2/D$ according to the periodic Anderson model picture [36], the critical concentration $c_{\text{imp}}^{\text{cr}}$ is roughly estimated as

$$c_{\text{imp}}^{\text{cr}} \sim \frac{8}{3} \left(\frac{V}{D} \right)^2 \frac{1}{N(0)D} \sim \frac{8}{3} \left(\frac{V}{D} \right)^2. \quad (41)$$

This is not extremely smaller than 1 in the usual situation for heavy Fermion metals. The result for the quantity $[-\text{Im}\Sigma_c^{\text{R}}(0, T) + \text{Im}\Sigma_c^{\text{R}}(0, 0)]/Dc_{\text{imp}}$ in Eq. (39) with the parameter set, $\tilde{V}/D = 0.4$, $\varepsilon_{\Gamma_3}/D = 0$, $\varepsilon_{\Gamma_7}/D = -0.4$, $\tilde{E}_0/D = 0.0821$, and $\tilde{a}_f = 0.339$, is shown in Fig. 5 for a series of c_{imp} , in which one can see that the coefficient of the T^2 term changes the sign at between $c_{\text{imp}} = 0.5$ and $c_{\text{imp}} = 0.6$. This is consistent with the experiment of the T dependence in the resistivity of $\text{Ce}_x\text{La}_{1-x}\text{Cu}_6$ [19, 20].

Furthermore, the critical concentration $c_{\text{imp}}^{\text{cr}} \sim 0.5$ in the single-channel impurities Anderson model is also consistent with the theoretical result of the T dependence in the resistivity of $\text{Ce}_x\text{La}_{1-x}\text{Cu}_6$ obtained with the use of the dynamical mean field theory (DMFT) and the coherent potential approximation (CPA) [29]. However, the result of Ref. [29] deviates from the Nordheim rule, $\rho \propto x(1-x)$, in the region $x < 0.2$ probably due to the difficulty of CPA when applied to the impurities Anderson model as mentioned in the last paragraph in §3. In addition, the T dependence in the resistivity in the two-channel lattice system and the two-channel impurities system cannot be explained by DMFT because the inter-site effect, which is crucial in the case of the two-channel Anderson models, lattice or impurities, is not taken into account in the formalism of DMFT.

Concluding this section, let us remark on the relation between the expression for A_{latt} [Eq. (31)] and Eq. (57) in Ref. [10]. According to the formula [Eq. (34)], the Fermi liquid component of the resistivity ρ_{FL} is given by

$$\rho_{\text{FL}} \approx \frac{2m}{N_e e^2} A_{\text{latt}} T^2. \quad (42)$$

Substituting the expression for A_{latt} [Eq. (31)] with the expression \tilde{C} [Eq. (23)], Eq. (42) is reduced to

$$\rho_{\text{FL}} = \frac{2m}{N_e e^2} \frac{\pi^3}{4N} \left(\frac{\tilde{a}_f V^2}{\tilde{E}_0} \right)^4 [N(0)]^2 \frac{\tilde{a}_f}{\tilde{E}_0^3} c_{\text{imp}}^2 T^2, \quad (43)$$

where $\tilde{a}_f(0)$ and $\tilde{E}_0(0)$ have been abbreviated by \tilde{a}_f and \tilde{E}_0 . With the use of approximate relations, $\tilde{E}_0 \sim \tilde{a}_f V^2/D$, $N(0)D \sim 1$, and $N(0) \sim N_F$, Eq. (43) is reduced to

$$\rho_{\text{FL}} = \left[\frac{2m}{N_e e^2} \frac{\pi^3}{4N} \left(\frac{D}{V} \right)^4 c_{\text{imp}}^2 \right] \pi N_F V^2 \frac{T^2}{\tilde{E}_0^2}. \quad (44)$$

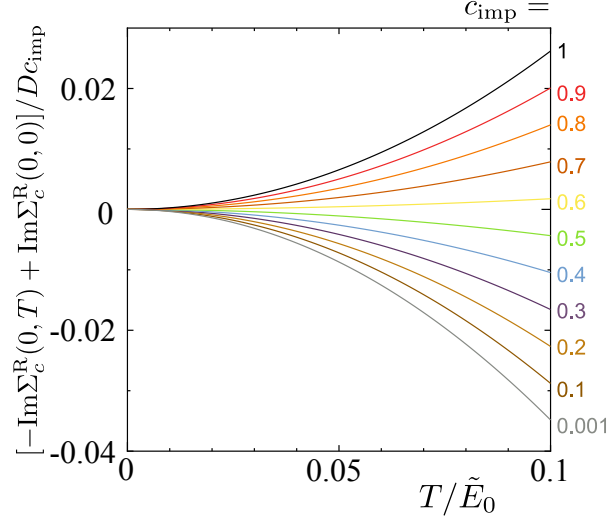


Figure 5. $[-\text{Im}\Sigma_c^R(0, T) + \text{Im}\Sigma_c^R(0, 0)]$ in Eq. (32) as a unit of Dc_{imp} for $M = 1$ with the parameter set, $\tilde{V}/D = 0.4$, $\varepsilon_{\Gamma_3}/D = 0$, $\varepsilon_{\Gamma_7}/D = -0.4$, $\tilde{E}_0/D = 0.0821$, and $\tilde{a}_F = 0.339$, as a function of T/\tilde{E}_0 for a series of $c_{\text{imp}} = 1 \sim 0.001$. The coefficient of T^2 dependence changes sign from positive to negative between $c_{\text{imp}} = 0.6$ and $c_{\text{imp}} = 0.5$ as decreasing the concentration c_{imp} , which is consistent with the observation reported in $\text{Ce}_x\text{La}_{1-x}\text{Cu}_6$ [19, 20].

Comparing this expression with that of Eq. (57) in Ref. [10], the factor in the brackets of Eq. (44) should be identified by a factor r in Eq. (57) of Ref. [10] for the bulk pure system, i.e., $c_{\text{imp}} = 1$.

7. Conclusion

We have shown theoretically that the two-channel Anderson impurities system as $\text{Y}_{1-x}\text{Pr}_x\text{Ir}_2\text{Zn}_{20}$ ($x = 0.024, 0.044, 0.085$, and 0.44) exhibits essentially the same non-Fermi liquid behaviors as the pure system with $x = 1$ unless x is extremely small less than $x^{\text{cr}} \sim 10^{-6}$ for a reasonable set of parameters. It was crucial to introduce a new formalism of treating the effect of random distribution of dilute Pr ions on virtual periodic lattice system. On this formalism, the theory for the lattice system can be applied with modifications of relevant parameters in the pure lattice system almost as it stands. In particular, the T dependence of the resistivity so calculated explains quite well that observed experimentally in diluted system $\text{Y}_{1-x}\text{Pr}_x\text{Ir}_2\text{Zn}_{20}$. The T dependence of other physical quantities, such as the specific heat, are also the same as those in periodic lattice systems. The critical impurities concentration $c_{\text{imp}}^{\text{cr}}$, below which the resistivity shows the temperature dependence of the single two-channel impurity model, has been shown to be extremely small not reached by controlled experiments, while that for the single-channel model is only moderately smaller than 1 in consistent with the observation in Ce-based impurity heavy fermion systems such as $\text{Ce}_x\text{La}_{1-x}\text{Cu}_6$.

Acknowledgments

We benefited much from stimulating conversations with K. Izawa, Y. Yamane and T. Onimaru for experimental aspects of the diluted Pr-1-2-20 system. This work is supported by the Grant-in-Aid for Scientific Research (No. 17K05555) from the Japan Society for the Promotion of Science.

Appendix A. Comment on Scaling Behavior of Temperature Dependence of Resistivity

In this appendix, we discuss the relationship between the T dependence of the resistivity $\rho(T)$ [Eq. (1)] and its scaling T dependence given by analyses of experiments for Pr-1-2-20 systems performed in Refs. [16, 17].

First, we should note that the definition of T_0 in Eq. (1) of the present paper is different from that of $T_0^{(\rho)}$ in Ref. [16] (and $T_0^{(17)}$ in Ref. [17]), in which $T_0^{(\rho)}$ (and $T_0^{(17)}$) are determined by the condition that the T dependence of the resistivity is scaled by $T_0^{(\rho)}$ (and $T_0^{(17)}$) with choosing the coefficient b (a_2 in their notation) appropriately. Here we have redefined “ T_0 ” in Ref. [17] as $T_0^{(17)}$ to distinguish it from T_0 defined in the present paper as the temperature where T dependence in $\rho(T)$ starts to apparently deviate from \sqrt{T} dependence. According to Fig. 3(a) in Ref. [17], $T_0^{(17)} \simeq T_0/0.45$ with $a_2 = 0.3$ for $\text{PrRh}_2\text{Zn}_{20}$ and $T_0^{(\rho)} \simeq T_0/0.75$ with $a_2 = 0.5$ for $\text{PrIr}_2\text{Zn}_{20}$, both of which correspond to taking $b \simeq 0.67$ and 0.67 , respectively, in Eq. (1). Note that the coefficient b 's for both cases are the same within experimental errors, supporting that the scaling behavior is universal.

Furthermore, the coefficient $b \simeq 0.67$ is also consistent with the theoretical expression [Eq. (1)] as seen in Fig. A1 in which two expressions, $T/(T + bT_0)$ and $\sqrt{T/T_0}/(1 + b)$, are drawn as a function of T/T_0 . Indeed, one can see that the theoretical expression $T/(T + bT_0)$ with $b = 0.67$ starts to apparently deviate from \sqrt{T} dependence at $T/T_0 \simeq 1.00$, which well mimics the behaviors observed in Refs. [16, 17] (see Fig 3(a) in Ref. [17]).

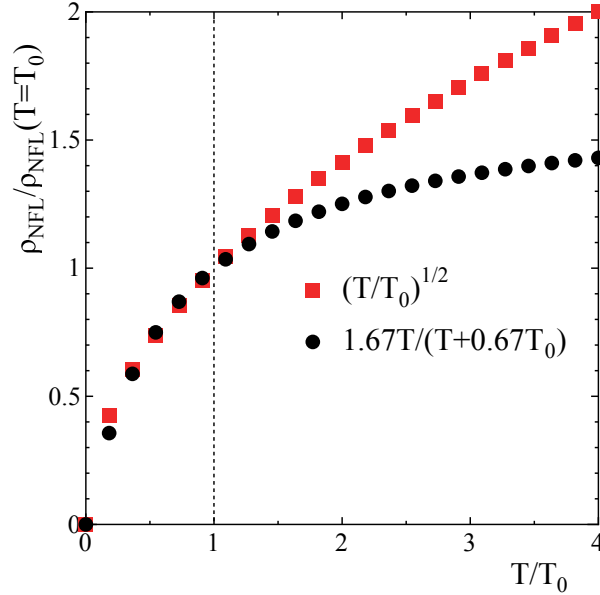


Figure A1. Black circles and red squares represent data points of the expression $T/(T + bT_0)$, the coefficient of the first term in Eq. (1) with $a = 1$ and $b = 0.67$, and those of the expression $\sqrt{T/T_0}/(1 + b)$, respectively. The abscissa is T/T_0 .

Concluding this appendix, we remark the relationship between the *approximate* expression [Eq. (1)], which is essentially the same as the second term in Eq. (59) in Ref. [10], and the numerical results for $\rho_{\text{NFL}}(T)$ given by Eq. (58) and shown in Fig. 11(b) of Ref. [10]. It is crucial to note that the characteristic temperature T_0 (denoted by T_0^{TM} hereafter) in Ref. [10] is defined as the temperature where $\rho_{\text{NFL}}(T)$ starts to apparently deviate from $(\text{const.} + \sqrt{T/D})$ behavior in Fig. 11(c), while T_0 of the present paper is defined as the temperature where it starts to apparently deviate from \sqrt{T} -like behavior without the “const.,” i.e., the offset introduced for extracting the component proportional to \sqrt{T} in Ref. [10]. In Fig. A2, the expression [Eq. (1)] with $b = 0.67$, and numerical result for $\rho_{\text{NFL}}(T)$ given by Eq. (58) and presented in Fig. 11(c) of Ref. [10], are shown as functions of T/T_0 instead of T/T_0^{TM} . One can see that both curves almost coincide with each other, implying that the scaling behaviors confirmed in $\text{PrRh}_2\text{Zn}_{20}$ [17] and $\text{PrIr}_2\text{Zn}_{20}$ [16] agree with the prediction given by Ref. [10].

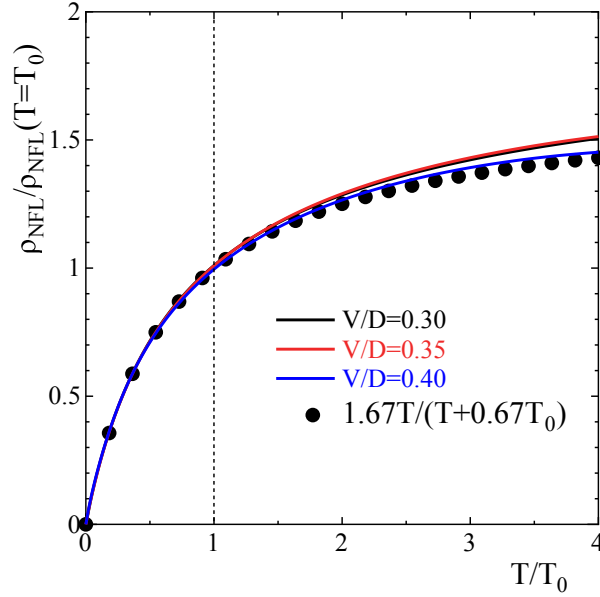


Figure A2. Relationship between *approximate* expression [Eq. (1)] with $b = 0.67$ (black circles) and numerical result for $\rho_{\text{NFL}}(T)$ given by Eq. (58) and presented in Fig. 11(c) of Ref. [10] for a series of c-f hybridizations $V/D = 0.30, 0.35$, and 0.40 . Note that the abscissa is T/T_0 and is different from T/T_0^{TM} in Fig. 11(c) of Ref. [10] as discussed in the text.

Appendix B. c-f Hybridization in *virtual* lattice system

In this appendix, we derive the hybridization term ($\equiv H_{\text{hyb}}^v$) in the *virtual* Hamiltonian [the 4th term in Eq. (12)] in the wave-vector representation. For the concise presentation, we introduce the operator $f_{i\tau\bar{\sigma}}^{\text{phy}} \equiv \tilde{b}_{i\tau}\tilde{f}_{i\sigma}^+$. Then, the hybridization term in the original Hamiltonian [Eq. (2)] is transformed by the average over the

random distribution of Pr ions to the following form:

$$H_{\text{hyb}}^{\text{v}} = \sum_{\sigma=1}^N \sum_{\tau=1}^M \sum_{\tilde{i}} V c_{i\tau\tilde{\sigma}}^+ f_{i\tau\tilde{\sigma}}^{\text{phy}} + \text{h.c.}, \quad (\text{B.1})$$

where \tilde{i} denotes the position on the *virtual* lattice. By a usual prescription, $f_{i\tau\tilde{\sigma}}^{\text{phy}}$ is expressed as

$$f_{i\tau\tilde{\sigma}}^{\text{phy}} = \frac{1}{\sqrt{N_{\text{f}}}} \sum_{\mathbf{p}} e^{i(\mathbf{p} \cdot \mathbf{R}_{\tilde{i}})} f_{\mathbf{p}\tau\tilde{\sigma}}^{\text{phy}}. \quad (\text{B.2})$$

On the other hand, conduction electrons are defined on the original lattice points as noted below Eq. (12). Therefore, $c_{i\tau\tilde{\sigma}}^+$ is given by $c_{\mathbf{p}\tau\tilde{\sigma}}^+$ defined on all the original lattice points, i.e., other than the *virtual* lattice points, so that it is written as

$$c_{i\tau\tilde{\sigma}}^+ = \frac{1}{\sqrt{N_{\text{L}}}} \sum_{\mathbf{p}} e^{-i(\mathbf{p} \cdot \mathbf{R}_{\tilde{i}})} c_{\mathbf{p}\tau\tilde{\sigma}}^+. \quad (\text{B.3})$$

As a result, substituting expressions [Eqs. (B.2) and (B.3)] into Eq. (B.1), the hybridization in the *virtual* system is given by

$$H_{\text{hyb}}^{\text{v}} = \sqrt{c_{\text{imp}}} \sum_{\sigma=1}^N \sum_{\tau=1}^M \sum_{\mathbf{p}} V c_{\mathbf{p}\tau\tilde{\sigma}}^+ f_{\mathbf{p}\tau\tilde{\sigma}}^{\text{phy}} + \text{h.c.}, \quad (\text{B.4})$$

where $c_{\text{imp}} = N_{\text{f}}/N_{\text{L}}$ is the concentration of Pr ions in the original lattice. Converting the wave vector representation into the real space one in the *virtual* lattice with the use of inverse Fourier transformation of Eqs. (B.2) and (B.3), the 4th term in Eq. (10) is recovered. The c_{imp} dependence of Eq. (B.4) is reasonable considering that the effect of localized Pr ions on the conduction electrons reflects the concentration of Pr ions, and is crucial for understanding the relative importance of the impurities effect and the lattice effect in the single-channel Anderson model where the coefficient of T^2 term changes the sign from negative to positive at $c_{\text{imp}} \sim 0.5$ when the concentration of f-electrons increases from $c_{\text{imp}} = 0$ to 1, i.e., from the local Fermi liquid to the heavy Fermi liquid behavior as discussed in Sect. 6.

Appendix C. Self-energy of conduction electrons in *virtual* system

In this appendix, we show how the imaginary part of the self-energies [Eqs. (17)-(19)] is calculated.

Appendix C.1. Self-energies of Fig. 3(a)

First, we discuss how the expressions for the self-energies shown in Fig. 3(a) are obtained. To this end, we first rewrite Eq. (17) as

$$\text{Im}\Sigma_{\text{c}}^{(a)R}(\varepsilon = 0; T) = -\tilde{C} + A_{\text{imp}}T^2 + 2\tilde{C}\tilde{a}_f(T/\tilde{E}_0)^\nu \left(1 - \frac{1}{M^2}\right), \quad (\text{C.1})$$

where $\nu \equiv (1 - \tilde{a}_f)\frac{M}{N}$.

The self-energy $\Sigma_{\text{c}}^{(a1)}(i\varepsilon_n)$ shown by the Feynman diagram of the first term in Fig. 3 (a) has no imaginary part, i.e., $\text{Im}\Sigma_{\text{c}}^{(a1)R}(\varepsilon = 0) = 0$ because $\Sigma_{\text{c}}^{(a1)}(i\varepsilon_n)$ is given as

$$\Sigma_{\text{c}}^{(a1)R}(i\varepsilon_n) = \frac{\tilde{a}_f V^2}{M} \frac{1}{i\varepsilon_n - \tilde{E}_0}, \quad (\text{C.2})$$

so that

$$\text{Im}\Sigma_c^{(a1)R}(\varepsilon) = -\pi \frac{\tilde{a}_f V^2}{M} \delta(\varepsilon - \tilde{E}_0). \quad (\text{C.3})$$

The self-energy $\Sigma_c^{(a2)}(i\varepsilon_n)$ shown by the Feynman diagram of the second term in Fig. 3(a) gives the terms, $-\tilde{C} + A_{\text{imp}}T^2$, in Eq. (C.1) as shown below. The explicit form of the self-energy $\Sigma_c^{(a2)}(i\varepsilon_n)$ is given by

$$\begin{aligned} \Sigma_c^{(a2)}(i\varepsilon_n) = \tilde{V}^4 T^2 \sum_{\omega_m, \omega_l} \frac{1}{N_L} \sum_{\mathbf{p}, \sigma} \bar{G}_{\mathbf{p}\tau\sigma}(-i\omega_m) \bar{F}_{i\sigma}(i\omega_l) \\ \times \bar{B}_{i\tau}^2(i\varepsilon_n + i\omega_l) \bar{F}_{i\sigma}(i\varepsilon_n + i\omega_l + i\omega_m) / \langle Q_i \rangle_\lambda, \end{aligned} \quad (\text{C.4})$$

where $\bar{G}_{\mathbf{p}\tau\sigma}(i\omega_n)$, $\bar{F}_{i\sigma}(i\omega_n)$, and $\bar{B}_{i\tau}(i\omega_n)$ have been given by Eqs. (49), (51), and (15) in Ref. 10, respectively. Substituting these expressions into Eq. (C.4), $\Sigma_c^{(a2)}(i\varepsilon_n)$ is reduced to

$$\begin{aligned} \Sigma_c^{(a2)}(i\varepsilon_n) = \frac{\tilde{a}_f^2(T) \tilde{V}^4}{N} \int d\varepsilon \tilde{N}(\varepsilon) \\ \times \left[\frac{f(-\varepsilon)}{(i\varepsilon_n - \tilde{E}_0(T))^2 (i\varepsilon_n - \varepsilon)} - \frac{f(\varepsilon)}{(\varepsilon - \tilde{E}_0(T))^2 (-i\varepsilon_n + \varepsilon)} \right], \end{aligned} \quad (\text{C.5})$$

where $\tilde{N}(\varepsilon) \equiv -(1/\pi N_f) \sum_{\mathbf{p}, \tau} \text{Im} \bar{G}_{\mathbf{c}\tau\sigma}^R(\mathbf{p}, \varepsilon)$, and $\tilde{E}_0(T)$ and $\tilde{a}_f(T)$ are solutions of Eqs. (24) and (25) at finite temperature. Thus, after simple calculations, the imaginary part of $\Sigma_c^{(a2)R}(\varepsilon = 0; T)$ is given as

$$\text{Im}\Sigma_c^{(a2)R}(0; T) = -\frac{\pi}{N} \left(\frac{\tilde{a}_f(T) \tilde{V}^2}{\tilde{E}_0(T)} \right)^2 \tilde{N}(0), \quad (\text{C.6})$$

in the low temperature range $0 \leq T \ll E_0$. At $T = 0$, it is reduced to

$$\text{Im}\Sigma_c^{(a2)R}(0; 0) = -\tilde{C}, \quad (\text{C.7})$$

where

$$\tilde{C} \equiv \frac{\pi}{N} \left(\frac{\tilde{a}_f(0) \tilde{V}^2}{\tilde{E}_0(0)} \right)^2 \tilde{N}(0), \quad (\text{C.8})$$

which is nothing but Eq. (21). The solutions of Eqs. (24) and (25) at finite temperature, $0 < T \ll E_0$, change from those at $T = 0$ as

$$\tilde{E}_0(T) = \tilde{E}_0(0) + \Delta \tilde{E}_0(T), \quad (\text{C.9})$$

$$\tilde{a}_f(T) = \tilde{a}_f(0) + \Delta \tilde{a}_f(T). \quad (\text{C.10})$$

Using the Sommerfeld expansion in Eqs. (24) and (25), we obtain the modifications $\Delta \tilde{E}_0(T)$ and $\Delta \tilde{a}_f(T)$ in the lowest order in T^2 as

$$\frac{\Delta \tilde{E}_0(T)}{\tilde{E}_0(0)} \simeq \frac{\pi^2}{6} [1 - \tilde{a}_f(0)] \left[\frac{T}{\tilde{E}_0(0)} \right]^2, \quad (\text{C.11})$$

$$\frac{\Delta \tilde{a}_f(T)}{\tilde{a}_f(0)} \simeq -\frac{\pi^2}{6} [1 - \tilde{a}_f(0)] [1 + \tilde{a}_f(0)] \left[\frac{T}{\tilde{E}_0(0)} \right]^2. \quad (\text{C.12})$$

Substituting these results into Eq. (C.6), we obtain A_{imp} in Eq. (C.1) as

$$\begin{aligned} A_{\text{imp}} &\equiv \lim_{T \rightarrow 0} \frac{1}{T^2} [\text{Im}\Sigma^{(a2)R}(0; T) - \text{Im}\Sigma^{(a2)R}(0; 0)] \\ &= \frac{\pi^2}{3} \tilde{C} [1 - \tilde{a}_f(0)] [2 + \tilde{a}_f(0)] \frac{1}{[\tilde{E}_0(0)]^2}, \end{aligned} \quad (\text{C.13})$$

which is nothing but Eq. (27).

The self-energy $\Sigma_c^{(a3)}(i\varepsilon_n)$ given by the Feynman diagrams of the terms illustrated as dots in Fig. 3 (a), which is the third term in Eq. (C.1), has the imaginary part

$$\text{Im}\Sigma_c^{(a3)R}(\varepsilon = 0; T) = 2\tilde{C}\tilde{a}_f(0)[T/\tilde{E}_0(0)]^\nu(1 - M^{-2}). \quad (\text{C.14})$$

The explicit form of the dots in Fig. 3 (a) is shown in Fig. 4 in Ref. [30], and that of $\text{Im}\Sigma_c^{(a3)R}(\varepsilon = 0; 0)$ is given by Eq. (4.6) in Ref. [30].

Appendix C.2. Self-energy of Fig. 3(b)

Second, we discuss why the self-energy $\Sigma_c^{(b)}(i\varepsilon_n)$ shown by the Feynman diagram of Fig. 3 (b) is necessary [37]. The Green function of the conduction electrons of the order of $O[(1/N)^0]$ consists of series of terms including power series of $\Sigma_{ci}^{(a1)}(i\varepsilon_n)$ as

$$\begin{aligned} \bar{G}_{\text{p}\tau\sigma}(i\varepsilon_n) &= \bar{G}_{\text{p}\tau\sigma}^0(i\varepsilon_n) + [\bar{G}_{\text{p}\tau\sigma}^0(i\varepsilon_n)]^2 \frac{1}{N_f} \sum_i \Sigma_i^{(a1)}(i\varepsilon_n) \\ &\quad + [\bar{G}_{\text{p}\tau\sigma}^0(i\varepsilon_n)]^3 \frac{1}{N_f^2} \sum_{i \neq j} \Sigma_i^{(a1)}(i\varepsilon_n) \Sigma_j^{(a1)}(i\varepsilon_n) + \dots, \end{aligned} \quad (\text{C.15})$$

where $\bar{G}_{\text{p}\tau\sigma}^0(i\varepsilon_n)$ is the bare Green function of the conduction electrons. The reason why only the terms $i \neq j$, etc., are taken into account is that the terms with $i = j$, etc., vanish after taking the limit $\{\lambda_i\} \rightarrow \infty$ in Eq. (4) for calculating expectation value of physical quantities. Since the series of higher order terms of $\Sigma_i^{(a1)}(i\varepsilon_n)$ cannot be collected as a form of self-energy as it stands, we rearrange these terms as

$$\begin{aligned} \bar{G}_{\text{p}\tau\sigma}(i\varepsilon_n) &= \bar{G}_{\text{p}\tau\sigma}^0(i\varepsilon_n) \left\{ 1 + \bar{G}_{\text{p}\tau\sigma}^0(i\varepsilon_n) \frac{1}{N_L} \sum_i \Sigma_i^{(a1)}(i\varepsilon_n) \right. \\ &\quad \left. + \left[\bar{G}_{\text{p}\tau\sigma}^0(i\varepsilon_n) \frac{1}{N_L} \sum_i \Sigma_i^{(a1)}(i\varepsilon_n) \right]^2 + \dots \right\} \\ &\quad - [\bar{G}_{\text{p}\tau\sigma}^0(i\varepsilon_n)]^2 \left[\frac{1}{N_L^2} \sum_i \sum_{\text{p}'} \bar{G}_{\text{p}'\tau\sigma}^0(i\varepsilon_n) \Sigma_i^{(a1)}(i\varepsilon_n) \Sigma_i^{(a1)}(i\varepsilon_n) + \dots \right], \end{aligned} \quad (\text{C.16})$$

where the first line can be collected as the self-energy $\frac{1}{N_L} \sum_i \Sigma_{ci}^{(a1)}(i\varepsilon_n)$. The self-energy $\Sigma_c^{(b)}(i\varepsilon_n)$ is defined by the expression in the bracket in the second line of Eq. (C.16), and its explicit form is given by

$$\begin{aligned} \Sigma_c^{(b)}(i\varepsilon_n) &= -\tilde{V}^4 T^2 \sum_{\omega_l, \omega_m} \frac{1}{N_L} \sum_{\text{p}, \sigma} \bar{G}_{\text{p}\tau\sigma}(i\varepsilon_n) \bar{F}_{i\sigma}(i\omega_l) \bar{B}_{i\tau}(i\varepsilon_n + i\omega_l) \\ &\quad \times \bar{F}_{i\sigma}(i\omega_m) \bar{B}_{i\tau}(i\varepsilon_n + i\omega_l) / \langle Q_i \rangle_\lambda^2. \end{aligned} \quad (\text{C.17})$$

Thus, after simple calculations, the imaginary part of $\Sigma_c^{(b)R}(0;0)$ is given as

$$\text{Im}\Sigma_c^{(b)R}(0;0) = \tilde{C} \frac{1}{M^2}, \quad (\text{C.18})$$

which is nothing but Eq. (18).

Appendix C.3. Self-energy of Fig. 3(c)

Finally, we discuss the self-energy $\Sigma_c^{(c)}(i\varepsilon_n)$ shown by the Feynman diagram of Fig. 3 (c). The explicit diagrams included in vertices Γ_{loc} and Γ in $\Sigma^{(c)}(i\varepsilon_n)$ are illustrated in Fig. C1 (a) and (b), respectively.

If we use $\Gamma_{\text{loc}}^{(0)}$ as the local vertex Γ_{loc} in Fig. C1 (b), the imaginary part of the self-energy, $\text{Im}\Sigma_c^{(c)R}(\varepsilon=0;T)$, is given by

$$\text{Im}\Sigma_c^{(c)R}(\varepsilon=0;T) = \tilde{C} \frac{1}{1 + \frac{\tilde{T}^{*(0)}}{T}} \frac{\tilde{T}^{*(0)}}{T} \left(1 - \frac{1}{M^2}\right) - A_{\text{latt}} T^2, \quad (\text{C.19})$$

as has been shown in discussions leading to Eq. (42) in Ref. 10. $T^{*(0)}$ in Eq. (C.19) is given by

$$T^{*(0)} = \frac{\tilde{E}_0}{1 + \tilde{N}(0)\tilde{E}_0}, \quad (\text{C.20})$$

which appears in the factor b of Eq. (59) in Ref. 10.

Following the method for deriving imaginary part of the self-energy of the Fermi liquid quasiparticles in Ref. [38], the coefficient A_{latt} is derived as

$$A_{\text{lattice}} = \frac{\pi}{4} \tilde{C}^2 N \frac{\tilde{a}_f(0)}{[\tilde{E}_0(0)]^3}, \quad (\text{C.21})$$

where we have approximated the full vertex $\Gamma(\vec{p}, \vec{p}_2; \vec{p}_1, \vec{p} + \vec{p}_2 - \vec{p}_1)$ appearing in Eq. (19.31) of Ref. [38] by $\Gamma^{\text{loc}(0A)}$, defined by Eq. (27) in Ref. [10] which is reduced to $2\tilde{a}_f^2 \tilde{V}^4 / M \tilde{E}_0^3$ in the static limit, and $p_0 v$ as $N \tilde{E}_0$ with $N = 2$. We have also assumed that the dispersion of the quasiparticles is given by that of the plane wave in three dimensions. Note that the expression for the coefficient A in Ref. [38] is reduced to

$$A = \frac{1}{4} \left| \frac{a_f^2 p_0}{\pi^2 v} \Gamma \right|^2 \quad (\text{C.22})$$

if the wave vector dependence of the vertex Γ is neglected.

The local vertex $\Delta\Gamma_{\text{loc}}^{1a}$ shown by the Feynman diagram of the *first* term in the *first* bracket in Fig. C1 (d) is given by

$$\begin{aligned} \Delta\Gamma_{\text{loc}}^{1a}(i\varepsilon_{n_1}, i\varepsilon_{n_2}; ix_l) &= -\frac{1}{N_f} \sum_{\mathbf{p}} T^2 \sum_{\nu_m, \omega_n} \bar{F}_{i\sigma}(i\nu_m) \bar{F}_{i\sigma}(i\nu_m + ix_l) \\ &\quad \times \bar{B}_{i\tau}(i\nu_n + i\varepsilon_{n_1}) \bar{F}_{i\sigma}^2(i\nu_m + i\varepsilon_{n_2}) \bar{G}_{\mathbf{p}\tau\sigma}(-i\omega_n) \\ &\quad \times \bar{B}_{i\sigma}(i\nu_m + i\varepsilon_{n_2} + i\omega_n) / \langle Q_i \rangle_{\lambda_i}, \end{aligned} \quad (\text{C.23})$$

where ε_{n_i} ($i = 1, 2$) are fermionic Matsubara frequencies and x_l and ν_m are bosonic Matsubara frequencies, respectively. After the analytic continuation from $i\varepsilon_{n_i}$ to $\varepsilon_i + i\delta$ and taking the limit ε_1 and $\varepsilon_2 \ll T$, $\Delta\Gamma_{\text{loc}}^{1a}$ [Eq. (C.23)] is reduced to

$$\Delta\Gamma_{\text{loc}}^{1a}(i\delta, i\delta; x_l) = -\frac{1}{T} \delta_{x,0} \tilde{N}(0) \left(\frac{\tilde{a}_f \tilde{V}^2}{\tilde{E}_0} \right)^3 \log \frac{T}{\tilde{E}_0}. \quad (\text{C.24})$$

Refer to Appendix A in Ref. [30] for an explicit calculation of the expression [Eq. (C.23)]. Similarly, the singular terms in each diagram in Fig. C1 (d) of the order of $O[(1/N)^n]$ is shown to be proportional to $[\log(T/\tilde{E}_0)]^n$ as can be seen in calculations performed in §4 of Ref. [30].

In the case of single-channel, $M = 1$, the singular terms cancel with each other, while in the case of multichannel, $M \geq 2$, the singular terms remain in the local vertex. Just as $\text{Im}\Sigma^{(a3)}$ includes singular factor $[T/\tilde{E}_0]^\nu$ in Eq. (C.14), the full local vertex $\Gamma_{\text{loc}}^{(B)}$ illustrated in Fig. C1 (d) includes the singular term proportional to $(T/\tilde{E}_0)^\nu$ as follows:

$$\begin{aligned} \Gamma_{\text{loc}}^{(B)}(i\delta, i\delta : ix_l) &= \frac{\tilde{a}_f^2 \tilde{V}^4}{\tilde{E}_0^2} \frac{1}{T} \delta_{x_l, 0} \left[1 - 2\tilde{a}_f(T/\tilde{E}_0)^\nu \right] \\ &\times (\delta_{\sigma_1, \sigma_4} \delta_{\sigma_2, \sigma_3} - M^{-1} \delta_{\sigma_1, \sigma_3} \delta_{\sigma_2, \sigma_4}), \end{aligned} \quad (\text{C.25})$$

which includes the higher order corrections in $(1/N)$ to $\Gamma^{(B)}$ in Eq. (29) of Ref. [10]. (See also Ref. [14] for the dependence on $\sigma_1, \sigma_2, \sigma_3, \sigma_4$.)

An explicit form of the Bethe-Salpeter equation illustrated in Fig. C1 (b) is given as

$$\begin{aligned} \Gamma_{\mathbf{q}}^{(B)}(i\delta, i\delta : ix_l) &= \Gamma_{\text{loc}}^{(B)}(i\delta, i\delta : ix_l) \\ &+ \Gamma_{\text{loc}}^{(B)}(i\delta, i\delta : ix_l) T \sum_{\varepsilon_n} \frac{1}{N_f} \sum_{\mathbf{p}} \bar{G}_{\mathbf{p}\tau\sigma}(i\varepsilon_n) \bar{G}_{\mathbf{p}+\mathbf{q}\tau\sigma}(i\varepsilon_n + ix_l) \\ &\times \Gamma_{\mathbf{q}}^{(B)}(i\delta, i\delta : ix_l). \end{aligned} \quad (\text{C.26})$$

By solving this equation, we obtain the full vertex $\Gamma_{\mathbf{q}}^{(B)}(i\delta, i\delta : ix_l)$ as follows:

$$\begin{aligned} \Gamma_{\mathbf{q}}^{(B)}(i\delta, i\delta : ix_l) &= \frac{\frac{1}{N(0)} \frac{T^{*(0)}}{T} \left[1 - 2\tilde{a}_f \left(\frac{T}{\tilde{E}_0} \right)^\nu \right]}{1 + \frac{T^{*(0)}}{T} \left[1 - 2\tilde{a}_f \left(\frac{T}{\tilde{E}_0} \right)^\nu \right]} \\ &\times (\delta_{\sigma_1, \sigma_4} \delta_{\sigma_2, \sigma_3} - M^{-1} \delta_{\sigma_1, \sigma_3} \delta_{\sigma_2, \sigma_4}) \delta_{x_l, 0}, \end{aligned} \quad (\text{C.27})$$

where the expression of the denominator is derived from the factor $K_{\mathbf{q}}(0)[K_{\mathbf{q}}(0) - T^{-1}f_{\mathbf{q}}^{(0,2)}(0)]$ in the denominator of Eq. (33) in Ref. [10], and that of the numerator is given by Γ_{loc} [Eq. (C.25)]. By calculating the self-energy in Fig. 3(c), we obtain the imaginary part of the self-energy $\Sigma_c^{(c)R}(\varepsilon = 0; T)$ as

$$\text{Im}\Sigma_c^{(c)R}(\varepsilon = 0; T) = \tilde{C} \frac{1 - 2\tilde{a}_f(T/\tilde{E}_0)^\nu}{1 + \frac{\tilde{T}^*}{T}} \frac{\tilde{T}^*}{T} \left(1 - \frac{1}{M^2} \right) - A_{\text{latt}} T^2, \quad (\text{C.28})$$

where \tilde{T}^* is given by

$$\tilde{T}^* = \tilde{T}^{*(0)} [1 - 2\tilde{a}_f(T/\tilde{E}_0)^\nu]. \quad (\text{C.29})$$

Equation (C.28) is nothing but Eq. (19).

- criticality, as discussed in K. Miyake and S. Watanabe, JPS Conf. Proc. **30**, 011027 (2020).
- [24] A. A. Abrikosov, L. P. Gor'kov, and I. Ye. Dzyaloshinskii, *Quantum Field Theoretical Methods in Statistical Physics* (Pergamon, Oxford, U.K., 1965) 2nd ed., Sect. 39.
- [25] T. Onimaru, private communications.
- [26] The manner of this splitting of conduction bands was verified in relation to explaining the impurities concentration dependence of the quadrupole ordering temperatures in Pr-1-2-20 impurities systems, which will be discussed elsewhere.
- [27] J. M. Ziman, *Models of disorder* (Cambridge 1979), Sect. 9.
- [28] T. Yanagisawa, H. Amitsuka, S. Zherlitsyn, J. Wosnitza, Y. Yamane, and T. Onimaru, Phys. Rev. Lett. **123**, 067201 (2019).
- [29] T. Mutou, Phys. Rev. B **64**, 245102 (2001).
- [30] A. Tsuruta, Y. Ōno, T. Matsuura and Y. Kuroda, J. Phys. Soc. Jpn. **67**, 2346 (1998).
- [31] This expression for ν is essentially the same as Eq. (4.6) in Ref. [30] in which $M \ll N$ has been assumed. However, the exact expression in the case of $M = N$ as in the present case, is expected to be $\nu \equiv (1 - \tilde{a}_f)M/(N + M)$ because this exponent was derived by the NCA (Non-Crossing Approximation) that is considered to be valid at the high- T region, $T > \tilde{E}_0(0) \sim T_K$, as discussed in Ref. [8]. Namely, in that case, the relation $\nu = 1/2$ holds when $N = M = 2$, which is consistent with the correct result in the two-channel Kondo model given in Ref. [11].
- [32] In Ref. [10], the factor $[1 - 2\tilde{a}_f(T/\tilde{E}_0)^\nu]$ in Eq. (32) has been approximated as 1 because they were interested in the T region, $T < \tilde{T}^* \sim \tilde{E}_0(0) \sim T_K$, where the factor $2\tilde{a}_f(T/\tilde{E}_0)^\nu$ gives only minor correction to the T dependence of $\text{Im}\Sigma_c^R(\varepsilon = 0, T)$.
- [33] Y. Yamane and T. Onimaru, private communications.
- [34] The spatial extent of the Kondo-Yosida singlet, ξ_{KY} , of the single-channel Kondo effect was estimated in K. Yosida and A. Yoshimori, Prog. Theor. Phys. **42**, 753 (1969), as $\xi_{KY} \sim (v_F/T_K)(JN_{cF})^2$ with v_F and $T_K \equiv D\sqrt{JN_{cF}}e^{-(1/JN_{cF})}$ being the Fermi velocity of conduction electrons and the Kondo temperature of the impurity system, respectively. Here, D , J and N_{cF} are half the bandwidth of conduction electrons, the c-f exchange interaction, and the DOS of conduction electrons per electron at the Fermi level, respectively. If we assume that $T_K \sim 10\text{K}$, $D \sim 10^4\text{K}$ and the dispersion of conduction electrons is given by that of the free electron, the ξ_{KY} is estimated as $\xi_{KY} \sim 5a$ with a being the mean distance among conduction electrons. For much more rigorous treatment was given in H. Ishii, J. Low Temp. Phys. **32**, 457 (1978) in which the magnetic correlation between local moment and conduction electrons decays in proportion to r^{-4} in the region $r \gtrsim \xi_{KY}$.
- [35] P. Nozières, J. Low Temp. Phys. **17**, 31 (1974).
- [36] T. M. Rice and K. Ueda, Phys. Rev. B **34**, 6420 (1986).
- [37] K. Miura, T. Matsuura and Y. Kuroda, Physica C **179** 411 (1991).
- [38] A. A. Abrikosov, L. P. Gor'kov, and I. Ye. Dzyaloshinskii, *Quantum Field Theoretical Methods in Statistical Physics* (Pergamon, Oxford, U.K., 1965) 2nd ed., Sect. 19.